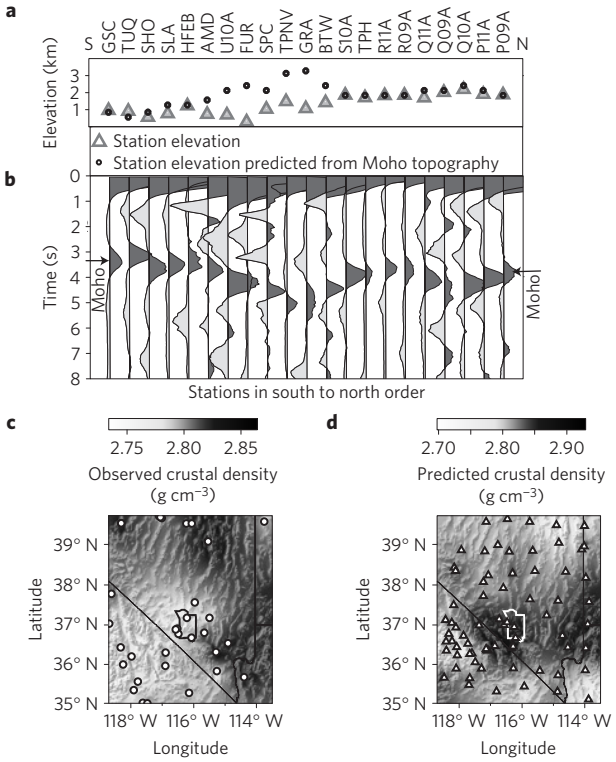

Figure 2 | Lack of isostatic compensation within the crust. a, North–south seismic station profile for stations shown in blue in Fig. 1b (selected to cross the anomaly; some noisier stations were omitted) with smoothed (to account for elastic plate thickness[27]) station elevations (grey triangles) and station elevations predicted from Moho topography (black circles, top) assuming isostatic compensation of the crust (see Supplementary Information). **b**, Station average radial receiver functions. **c**, Observed average crustal density scaled from refraction study (circles) P velocities[3]. **d**, Predicted average crustal density from forcing isostatic compensation within the crust while matching Moho delay times at stations (triangles).

Figure 1 | Location of study area, topography and Moho depths. **a**, Topographic overview map with the study area outlined in blue and tectonic provinces in red. **b**, Topographic map of the study area (note the elevation drop from northern to central Basin and Range). The yellow line is the western edge of the Precambrian craton based on Sr, Nd, and U–Pb isotope studies[28–30]. Faults in blue; Nevada Test Site outlined in black for orientation in subsequent plots. **c**, Moho depth determined from receiver functions (delay times converted to depth using crustal velocities from refraction experiments[3]). Moho is interpolated between values at stations (triangles; stations used in Fig. 2a,b in blue).

in Fig. 3a) projected on a north–south profile. The purely thermal density contrast for this composition would be sufficient to explain surface elevation with a lithospheric root thickness of ~100 km or slightly less (Fig. 3c). However, the lithosphere is probably depleted in major elements relative to the asthenosphere, which reduces its density (for example, by ~0.05 g cm^{-3} for a depleted harzburgite endmember model; see Supplementary Information). The reduction of lithospheric density reduces the amount by which it decreases surface elevation (see Methods, equation (3)), therefore a deeper lithospheric root is needed if it is depleted. Further constraints on the state of the mantle are provided by the observed basaltic magmatism. As there is recent small-volume basaltic magmatism in the area of the root (Fig. 3a,d,e), the geotherm must be in the vicinity of the solidus at some depth. For the asthenospheric composition in Fig. 3b, the geotherm crosses the solidus at 50 km depth. Solidus temperatures increase with major element depletion (see Supplementary Information). Melting in the presence of a much thicker lithosphere requires high asthenospheric temperatures[19] that would put the shallower asthenosphere in the vicinity of the mantle root, well above the solidus (Fig. 3b), resulting in widespread and large-volume volcanism, which is not observed. Hydration or metasomatic enrichment of the lithosphere are mechanisms by which melting can occur at lower temperatures. Direct determination of melting depths and temperatures is difficult, as the erupted basalts are not primary melts (see Supplementary Information). Tomographic images[20,21] show no clear relation to the lithospheric root (see Supplementary Information), which excludes a simple temperature-dependent velocity–density scaling and suggests compositional heterogeneity or the presence of partial melt.

A compositionally distinct lithospheric root is also suggested by the very unusual geochemical signature observed within the area of the antibuoyant mantle[7]. Small-volume basaltic magmatism occurs across most of the study area (Fig. 3a). However, the area of the density anomaly alone yields basalts with very low ε_{Nd} values persisting to present day (Fig. 3d,e). Low ε_{Nd} values in basalts

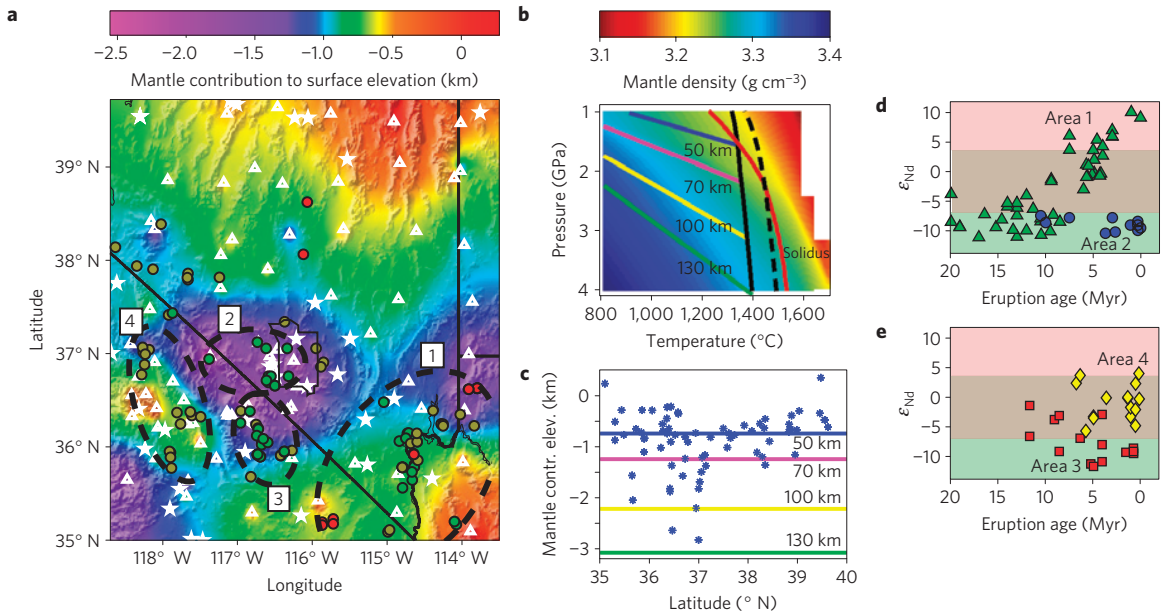

Figure 3 | Mantle buoyancy and basalt geochemistry. a, Map of lithospheric mantle contribution to observed surface elevation. White triangles, station locations; white stars, refraction results. Circles are basalts[6–11] from enriched lithospheric ($\varepsilon_{Nd} < -7$, green), asthenospheric ($\varepsilon_{Nd} > 4$, red), and intermediate (brown) mantle sources. **b**, pMELTS (ref. 17) mantle densities for an average asthenospheric composition[18] and adiabatic (solid black, $T_{pot} = 1{,}300\,^{\circ}C$; dashed, $T_{pot} = 1{,}390\,^{\circ}C$) and conductive geotherms (50–130 km lithospheric thickness); solidus in red. **c**, Predicted (coloured lines) mantle contribution to surface elevation from integration along geotherms ($T_{pot} = 1{,}300\,^{\circ}C$) in **b** compared to observed values (blue stars) at each station shown in **a**, S–N profile. **d**,**e**, Time progression[6] of basalt ε_{Nd} values in areas marked in **a**.

require a long-lived mantle reservoir that has been enriched with trace elements over a long time, whereas basalts derived from convecting asthenosphere have positive ε_{Nd}. Values in basalts of −10 and lower, such as found above the inferred lithospheric root, require that 100% of the Nd in the sample originated in enriched lithospheric mantle[7,8,22]. In the western US, such low values in basalts are only found in the central Basin and Range and otherwise only much further east under Archaean cratons[7]. Within the central Basin and Range, basalts in the Lake Mead extensional area in the east have shifted from similarly low values to asthenospheric values (Area 1, Fig. 3a,d), interpreted as lithospheric removal[6]. Low ε_{Nd} basalts have persisted in the Death Valley extensional area in the west from 12 to 0 Myr ago (Area 2, Fig. 3a,d), with a distribution that matches the geographical extent of the lithospheric root (Fig. 3a). At the southern edge of the lithospheric root, ε_{Nd} values show an unusual decrease with time (Area 3, Fig. 3a,e), implying a shift from a less-enriched lithospheric or mixed lithospheric and asthenospheric source component to an enriched lithospheric mantle source[8]. West of the lithospheric root, ε_{Nd} values show a constant intermediate range (Area 4, Fig. 3a,e).

A pre-extension Precambrian-age lithosphere is likely to be present under the central Basin and Range, based on crustal basement ages (Fig. 1a). The crust (and presumably mantle) north of 37° N and west of 116° W is much younger (Palaeozoic[3]). The Mojave south of 36° N has Precambrian crust, but its lithosphere was modified and eroded during Laramide flat slab subduction, with a northern boundary roughly coinciding with the present day location of the Garlock Fault[23] (Fig. 4). We propose the history illustrated in Fig. 4: (1) An older, thicker, colder lithosphere underlies the central Basin and Range before the beginning of Cenozoic extension. Its presence delays the onset of extension compared to the northern and southern Basin and Range[1], and also prevents the large-volume ignimbrite volcanism prevalent in the northern and southern provinces[5]. (2) When extension initiates in the east, the lithospheric root moves westwards relative to the Colorado Plateau, and the upper crust and mantle beneath the Lake Mead domain

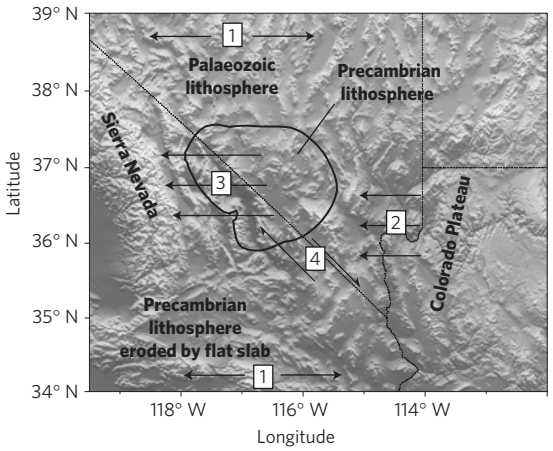

Figure 4 | Tectonic history. Inferred tectonic history sketched on a topographic map (motion arrows not to scale). The black closed shape is the −1 km contour from Fig. 3a (~present day location of lithospheric root). (1) (30–16 Myr; ref. 1) Extension and ignimbrite volcanism in the north and south, hindered by thick Precambrian lithosphere in the central Basin and Range. (2) (16–10 Myr; ref. 1) Breakaway of the root from Colorado Plateau to the west, extension in the Lake Mead domain. (3) (15–0 Myr; ref. 2) Lithospheric root left behind as top-to-west extension in the upper crust jumps to the Death Valley domain. (4) (13–0 Myr; ref. 24) Strike-slip motion carries southern Death Valley upper crust atop Precambrian lithospheric mantle.

undergo concurrent thinning. (3) However, when surface extension then jumps to the western corridor[2], the lithospheric mantle root maintains its position and is left behind while the overlying crust of the Death Valley domain undergoes top-to-the-west extension. (4) Finally, strike-slip motion initiates in the Walker Lane and Eastern California Shear Zone. Along the Stateline fault system east of Death Valley, 30 km of right-lateral offset has been inferred since

13 Myr ago[24]. The distance corresponds to the width of the area that shows decreasing ε_{Nd} values from 12 Myr ago to the present day (Area 3 in Fig. 3a,e). The lithospheric mantle is therefore decoupled from the east–west extension reaching across Death Valley and Panamint and Owens valleys to the Sierra Nevada, as well as from the right-lateral strike-slip motion and north–south shortening in the Walker Lane—Eastern California Shear Zone—Stateline Fault system. Increased lateral warming of the root may result in small-volume basaltic volcanism and gravitational instability[25], similar to the west for the Sierra Nevada, where lithospheric foundering is proposed to have caused uplift of the southern range[26].

Decoupling between the surface and mantle has been proposed for a portion of the northern Basin and Range, ~200 km north of our study area, based on GPS data[4]. Lithospheric thinning under the Lake Mead extensional domain and lateral offset between lithospheric and upper crustal extension in the Death Valley domain were proposed previously based on basalt geochemistry[6]. Two-dimensional lithospheric thickness profiles based on basalt melting depths[6,19] have arrived at lithospheric volumes that require the addition of lithospheric material from outside the central Basin and Range ('distributed shear'[6]), or imply extremely thick pre-extension lithosphere. Our three-dimensional model including decoupling between lithospheric mantle and upper crust and north–south shortening due to strike-slip motion removes some of the lithospheric volume balance problems. Our results present a picture of continental lithospheric deformation that is highly incoherent vertically as well as laterally, where upper crustal deformation can be controlled by pre-existing heterogeneity of strength in the mantle, but can also undergo decoupling from deeper structure, with both processes operating in succession in the same portion of lithosphere.

Methods

Seismic data sets for receiver function analysis were: (1) all broadband data available at the IRIS Data Management Center within the study area, including permanent stations, PASSCAL experiments, and EarthScope Transportable Array stations, from the years 1993–2008; (2) broadband and short-period data from the Southern Great Basin Digital Seismic Network over the years 2000–2007. P arrivals from teleseismic events with a magnitude of $m_b = 5.1$ or greater and within an epicentral range of 28°–99° were selected by a signal-to-noise ratio of the P onset on the vertical component of 3 or above. The time window used in the deconvolution was 20 s before to 30 s after the predicted direct P arrival. We calculated radial and tangential component receiver functions using a time-domain iterative method[13] with a Gaussian filter parameter of three and a minimum variance reduction cutoff of 70%. The results were hand sifted by event and after sorting by azimuth at each station, and we removed radial receiver functions lacking a positive direct P arrival at zero delay and any receiver functions with very large amplitudes or conversions lacking a zero crossing over more than 2.5 s. Results for representative stations are shown in the Supplementary Information. The Moho depths that we obtained by migrating the receiver function Moho delay times with P velocities interpolated between refraction experiment average values[3] and V_p/V_s of 1.73 (Fig. 1c) largely match refraction Moho depths, where those are available (see Supplementary Information).

To predict smoothed station elevations (Fig. 2a) from the Moho delay time observed at the station, we proceeded as follows. If the crust is in isostatic equilibrium, surface topography (T_S) scales to Moho topography (T_M) as $T_S = T_M/C$, where C is the density contrast $\rho_{crust}/(\rho_{mantle} - \rho_{crust})$. A range of crustal densities from 2.73 to 2.8 g cm^{-3} and mantle densities from 3.2 to 3.24 g cm^{-3} only results in variations of a few 100 m in predicted surface elevation, which is much smaller than the discrepancy to actual smoothed surface elevation of >2 km. We choose the most conservative estimate for T_S within the density ranges for mantle and crust. The above isostatic relation only predicts topography, and not absolute elevation. Matching the predicted to the observed elevation for stations with average Moho delay time results in a good fit everywhere except for the anomaly. Choosing different velocities and V_p/V_s ratios for converting Moho delay times to Moho depths has a small effect on the predicted topography, with the anomaly persisting, because changes in velocities and V_p/V_s affect absolute Moho depth to first order but change Moho topography only to second order. The effective elastic thickness of the lithosphere in the Basin and Range is reported as 1.5–15 km (ref. 27), therefore surface elevations should be compensated isostatically when smoothed over a small radius (here, 30 km; using a 50 km radius changes calculated lithospheric thickness insignificantly (<10 km)).

To calculate the crustal and lithospheric mantle contribution to surface topography, we express the smoothed surface elevation ε as the sum of crustal and mantle contributions[3,16], with a constant to bring it into a reference frame at a mid-ocean ridge (2.4 km; ref. 16):

$$\varepsilon = H_{crust} + H_{lithosphere} - H_0 \quad (1)$$

The elevation contribution of each layer is calculated from its thickness L and density ρ:

$$H_{crust} = L_{crust} * (\rho_{asthenosphere} - \rho_{crust})/\rho_{asthenosphere} \quad (2)$$

$$H_{lithosphere} = L_{lithosphere} * (\rho_{asthenosphere} - \rho_{lithosphere})/\rho_{asthenosphere} \quad (3)$$

For Fig. 2d, (lateral crustal variation required to explain the surface elevation with no mantle contribution), we hold lithospheric mantle thickness and density contrast in equation (3) constant. Equation (2) is substituted into equation (1), with the crustal thickness in equation (2) expressed as:

$$L_{crust} = z_{Moho} + \varepsilon \quad (4)$$

$$z_{Moho} = t_{Moho}/(1/v_s - 1/v_p) \quad (5)$$

$$v_p = a + b * \rho_{crust} \quad (6)$$

where z_{Moho} is the Moho depth, t_{Moho} the Moho S-P delay time from receiver functions, v_p the compressional seismic velocity, v_s the shear velocity, and equation (6) a linear velocity–density relationship for crustal materials[15]. We substitute equations (6)–(4) and (2) into equation (1), fix the v_p/v_s ratio to 1.73, and solve the resulting quadratic equation for the average crustal density ρ_{crust} required to satisfy crustal isostasy beneath each seismic station. Parameters for the velocity–density relationship vary with pressure, and therefore with depth, but we found little effect on the result from choosing relations valid for 20 km depth when compared to those for 40 km depth.

To calculate the lithospheric contribution to surface elevation (Fig. 3a), we solve equation (1) for $H_{lithosphere}$. The crustal contribution is calculated using densities scaled from refraction velocities (Fig. 2c). Using a constant average crustal density results in a very similar lithospheric mantle contribution (see Supplementary Information).

Received 2 December 2010; accepted 8 July 2011; published online 14 August 2011

References

1. McQuarrie, N. & Wernicke, B. P. An animated tectonic reconstruction of southwestern North America since 36 Ma. *Geosphere* **1,** 147–172 (2005).
2. Snow, J. & Wernicke, B. Cenozoic tectonism in the Central Basin and Range: Magnitude, rate, and distribution of upper crustal strain. *Am. J. Sci.* **300,** 659–719 (2000).
3. Jones, C. *et al.* Variations across and along a major continental rift—an interdisciplinary study of the Basin and Range province, western USA. *Tectonophysics* **213,** 57–96 (1992).
4. Wernicke, B., Davis, J., Niemi, N., Luffi, P. & Bisnath, S. Active megadetachment beneath the western United States. *J. Geophys. Res.* **113,** B11409 (2008).
5. Eaton, G. The Basin and Range province—origin and tectonic significance. *Annu. Rev. Earth Planet. Sci.* **10,** 409–440 (1982).
6. DePaolo, D. & Daley, E. Neodymium isotopes in basalts of the southwest Basin and Range and lithospheric thinning during continental extension. *Chem. Geol.* **169,** 157–185 (2000).
7. Farmer, G. *et al.* Isotopic evidence on the structure and origin of subcontinental lithospheric mantle in southern Nevada. *J. Geophys. Res.-Solid Earth* **94,** 7885–7898 (1989).
8. Asmerom, Y., Jacobsen, S. & Wernicke, B. Variations in magma source regions during large-scale continental extension, Death Valley region, western United States. *Earth Planet. Sci. Lett.* **125,** 235–254 (1994).
9. Feuerbach, D., Smith, E., Walker, J. & Tangeman, J. The role of the mantle during crustal extension—constraints from geochemistry of volcanic rocks in the Lake Mead area, Nevada and Arizona. *Geol. Soc. Am. Bull.* **105,** 1561–157 (1993).
10. Vaniman, D., Crowe, B. & Gladney, E. Petrology and geochemistry of hawaiite lavas from Crater Flat, Nevada. *Contrib. Mineral. Petrol.* **80,** 341–357 (1982).
11. Rogers, N., Hawkesworth, C. & Ormerod, D. Late Cenozoic basaltic magmatism in the western Great Basin, California and Nevada. *J. Geophys. Res.-Solid Earth* **100,** 10287–10301 (1995).
12. Saltus, R. & Thompson, G. Why is it downhill from Tonopah to Las Vegas? A case for mantle plume support of the high northern Basin and Range. *Tectonics* **14,** 1235–1244 (1995).
13. Ligorria, J. & Ammon, C. Iterative deconvolution and receiver-function estimation. *Bull. Seismol. Soc. Am.* **89,** 1395–1400 (1999).

14. Steinberger, B., Schmeling, H. & Marquart, G. Large-scale lithospheric stress field and topography induced by global mantle circulation. *Earth Planet. Sci. Lett.* **186,** 75–91 (2001).
15. Christensen, N. & Mooney, W. Seismic velocity structure and composition of the continental-crust—a global view. *J. Geophys. Res.-Solid Earth* **100,** 9761–9788 (1995).
16. Lachenbruch, A. & Morgan, P. Continental extension, magmatism and elevation—formal relations and rules of thumb. *Tectonophysics* **174,** 39–62 (1990).
17. Ghiorso, M., Hirschmann, M., Reiners, P. & Kress, V. The pMELTS: A revision of MELTS for improved calculation of phase relations and major element partitioning related to partial melting of the mantle to 3 GPa. *Geochem. Geophys. Geosyst.* **3,** 1030 (2002).
18. Workman, R. & Hart, S. Major and trace element composition of the depleted MORB mantle (DMM). *Earth Planet. Sci. Lett.* **231,** 53–72 (2005).
19. Wang, K., Plank, T., Walker, J. & Smith, E. A mantle melting profile across the Basin and Range, SW USA. *J. Geophys. Res.-Solid Earth* **107,** 2017 (2002).
20. Biasi, G. P. Lithospheric evolution of the Pacific-North American Plate Boundary considered in three dimensions. *Tectonophysics* **464,** 43–59 (2009).
21. Schmandt, B. & Humphreys, E. Seismic heterogeneity and small-scale convection in the southern California upper mantle. *Geochem. Geophys. Geosyst.* **11,** Q05004 (2010).
22. Yogodzinski, G., Naumann, T., Smith, E., Bradshaw, T. & Walker, J. Evolution of a mafic volcanic field in the central Great Basin, south central Nevada. *J. Geophys. Res.-Solid Earth* **101,** 17425–17445 (1996).
23. Luffi, P., Saleeby, J. B., Lee, C-T. A. & Ducea, M. N. Lithospheric mantle duplex beneath the central Mojave Desert revealed by xenoliths from Dish Hill, California. *J. Geophys. Res.-Solid Earth* **114,** B03202 (2009).
24. Guest, B., Niemi, N. & Wernicke, B. Stateline fault system: A new component of the Miocene-Quaternary Eastern California shear zone. *Geol. Soc. Am. Bull.* **119,** 1337–1346 (2007).
25. Elkins-Tanton, L. T. Continental magmatism, volatile recycling, and a heterogeneous mantle caused by lithospheric gravitational instabilities. *J. Geophys. Res.-Solid Earth* **112,** B03405 (2007).
26. Zandt, G. *et al*. Active foundering of a continental arc root beneath the southern Sierra Nevada in California. *Nature* **431,** 41–46 (2004).
27. Lowry, A., Ribe, N. & Smith, R. Dynamic elevation of the Cordillera, western United States. *J. Geophys. Res.-Solid Earth* **105,** 23371–23390 (2000).
28. Kistler, R. & Peterman, Z. Variations in Sr, Rb, K, Na, and initial Sr-87-Sr-86 in mesozoic granitic rocks and intruded wall rocks in Central California. *Geol. Soc. Am. Bull.* **84,** 3489–3511 (1973).
29. Farmer, G. & DePaolo, D. Origin of Mesozoic and Tertiary granite in the western United States and implications for pre-Mesozoic crustal structure: 2. Nd and Sr isotopic studies of unmineralized and Cu-mineralized and Mo-mineralized granite in the Precambrian craton. *J. Geophys. Res.* **89,** 141–160 (1984).
30. Coleman, D., Barth, A. & Wooden, J. Early to Middle Proterozoic construction of the Mojave province, southwestern United States. *Gondwana Res.* **5,** 75–78 (2002).

Acknowledgements

We thank P. Luffi for providing density, entropy, and thermobarometry calculations; B. Schmandt for providing a tomographic model; G. L. Farmer for discussions; B. Wernicke for comments; A. Dean, M. Pettit, J. Ball and C. Vockrodt for assistance with data processing and plots; and the US National Science Foundation for support. A. Dean and M. Pettit were funded in part by the Incorporated Research Institutions for Seismology's summer internship program. Maps were produced with GMT.

Author contributions

A.S. and G.B. initiated the seismic data exchange. G.B. contributed SGBDSN data and tomographic models. A.S. assisted with initial seismic data acquisition and analysis. C.J. pointed out the geographic correspondence between the isostatic results and basalt geochemistry and contributed the compilation of refraction experiment results. V.S-P. performed the seismic and isostatic analysis and wrote the paper. All authors discussed the results and commented on the paper.

Additional information

The authors declare no competing financial interests. Supplementary information accompanies this paper on www.nature.com/naturegeoscience. Reprints and permissions information is available online at http://www.nature.com/reprints. Correspondence and requests for materials should be addressed to V.S-P.